Journal Article

Enhancing fucoxanthin bioavailability: Octyl-modified maltodextrin micelles and ultrasound-assisted encapsulation

Han, L., Nong, M., Yang, J., Cao, J., Hu, B and Williams, P.A

Recommended citation:

Han, L., Nong, M., Yang, J., Cao, J., Hu, B and Williams, P.A (2026), 'Enhancing fucoxanthin bioavailability: Octyl-modified maltodextrin micelles and ultrasound-assisted encapsulation', Food Hydrocolloids, 178, 112641. doi: 10.1016/j.foodhyd.2026.112641

Food Hydrocolloids 178 (2026) 112641

Contents lists available at ScienceDirect

Food Hydrocolloids

journal homepage: www.elsevier.com/locate/foodhyd

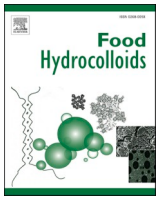

Enhancing fucoxanthin bioavailability: Octyl-modified maltodextrin micelles and ultrasound-assisted encapsulation

Lingyu Han [a,1], Mengsi Nong [a,1], Jixin Yang [b], Jijuan Cao [a], Bing Hu [a,*], Peter A. Williams [b,**]

[a] College of Life Science, Dalian Minzu University, Dalian, Liaoning, 116600, China
[b] Faculty of Life and Social Sciences, Wrexham University, Plas Coch, Mold Road, Wrexham, LL11 2AW, United Kingdom

ARTICLE INFO

Keywords:
Maltodextrin
Hydrophobic modification
Fucoxanthin
Ultrasound-assisted encapsulation
Micellar-like aggregates

ABSTRACT

Micelles are nanostructures capable of encapsulating hydrophobic substances within their hydrophobic cores, enabling their dispersion in aqueous media. This enhances the solubility, stability, and bioavailability of encapsulated bioactive compounds and allows for their controlled release. In this study, maltodextrin chains were chemically modified by adding hydrophobic octyl groups onto their backbone through an esterification reaction. As the degree of substitution increased, both the particle size of the micellar-like aggregates and the critical aggregation concentration (CAC) gradually decreased. The encapsulation efficiency and loading capacity exhibited a positive correlation with the degree of substitution. Furthermore, ultrasonic treatment, by inducing a cavitation effect, was found to enhance hydrophobic interactions within the micelles and significantly improve the encapsulation capacity and compensate for the lower degree of substitution. It also improved composite properties and imparted environmental stability to the micelle-like aggregates. *In vitro* modeling of the digestive process demonstrated that fucoxanthin-loaded micelle-like aggregates can effectively avoid gastric release while showing significantly enhanced intestinal release. As expected, the octyl-modified maltodextrin (MD-C8) markedly improved the bioaccessibility of fucoxanthin (49.57%) and increased the micellization rate (90.96%) during simulated gastrointestinal digestion. These findings indicate that MD-C8 is an effective delivery carrier for functional biomolecules. Combined with the approach of ultrasound-assisted techniques, it shows great potential for the applications in the encapsulation of hydrophobic compounds.

1. Introduction

Fucoxanthin is a naturally occurring carotenoid that is primarily derived from edible marine algae. It constitutes more than 10% of all naturally occurring carotenoids and functions as a primary pigment in marine ecosystems (Zhao et al., 2022). Fucoxanthin features a unique conjugated double bond system (resonance structure) as well as several oxygen-containing functional groups. Owing to its relatively low molecular weight, fucoxanthin can also be easily absorbed by living organisms. Moreover, fucoxanthin has shown no toxicity to human skin, liver, kidneys, spleen, and reproductive tissues and thus has diverse applications (Xiao et al., 2020). Functionally, fucoxanthin exhibits a range of biological activities, including antioxidant, anti-inflammatory, anti-obesity, and cardiovascular protective effects. As a result, fucoxanthin is highly suitable for incorporation into food, pharmaceutical, and cosmetic products. In practical applications, fucoxanthin can also be used as a nutritional supplement in functional foods to help prevent or mitigate chronic and age-related diseases (Zhang et al., 2024). Despite these advantages, the interconnected structure of fucoxanthin's polyene chains renders it chemically unstable and prone to oxidation in the presence of heat, light, and extreme pH levels. These environmental stresses can induce trans-cis isomerization, leading to a substantial decline in the bioavailability and efficacy of fucoxanthin. Consequently, fucoxanthin is vulnerable to alterations during processing, storage, and digestion, which limits its commercial applications (Tian et al., 2025). Additionally, interactions with hydrophobic functional molecules can further reduce the solubility of fucoxanthin in digestive fluids, further impairing its bioavailability (Xu et al., 2024).

In recent years, encapsulation technologies wherein the biological functionality of carotenoids is enhanced by improving their solubility

* Corresponding author.
** Corresponding author.
E-mail addresses: hubing19871121@163.com (B. Hu), Pete.Williams@wrexham.ac.uk (P.A. Williams).
[1] The authors contributed equally to this work.

https://doi.org/10.1016/j.foodhyd.2026.112641
Received 10 November 2025; Received in revised form 23 February 2026; Accepted 4 March 2026
Available online 5 March 2026

and stability have gained considerable attention (Kuang et al., 2024). The micellar-like aggregates used in drug delivery systems offer advantages such as enhanced bioavailability, improved solubility, and sustained release profiles (Thongpon et al., 2025). Given the abundance of diverse polysaccharides in natural biological systems, the chemical modification of these macromolecules has become a key area of research in materials science (Suenaga et al., 2025). Maltodextrin (MD) is a widely used polysaccharide that is derived from the partial hydrolysis of starch and has a higher affinity to water than most other carbohydrates (Sahiner et al., 2024). MD is recognized as an effective encapsulating carrier for a variety of substances, primarily due to its high-water solubility, low viscosity, and neutral taste. For instance, Sia et al. (2025) explored the preparation of microcapsules via spray-drying, using 15% MD as the encapsulating agent for anthocyanins extracted from jaboticaba juice. The resulting microcapsules achieved an encapsulation efficiency of 65%, demonstrating the feasibility of this method in preserving sensitive anthocyanin compounds. Similarly, Sahiner et al. (2024) employed MD and the crosslinker divinyl sulfone to prepare amoxicillin microcapsules via a reverse micelle crosslinking technique, achieving an encapsulation efficiency of 63.4 ± 4.1%. In another study, Kim et al. (2025) enhanced the stability of whey protein isolate (WPI) emulsions by applying a chitosan (CS) coating combined with spray-drying using MD or gum arabic (GA). This approach improved encapsulation efficiency from 75–78% to 95–98%. Notably, MD not only improves encapsulation efficiency but also contributes to optimizing particle size distribution and enhancing the storage stability of microcapsules. These advantages are typically dependent on its concentration, which can be fine-tuned to protect and deliver bioactive compounds. However, the spray-drying process used for preparing emulsions is relatively complex and often requires substantial amounts of oil to generate the dispersed phase. In contrast, micelle formation via the self-assembly of amphiphilic molecules in aqueous solutions represents a simplified approach. This method does not require complex equipment and instead utilizes molecular self-assembly mechanisms to form micellar systems, providing a more convenient and scalable strategy for the encapsulation and delivery of functional ingredients (Han et al., 2024).

Nevertheless, micellar-like aggregates systems still have some limitations in terms of encapsulation efficiency and bioavailability. For example, in a previous study, lipopolysaccharide (LPS) micelles derived from *E. coli* O113 demonstrated encapsulation efficiencies of 83%, 80%, 76%, and 74% for chloroquine (CQ), curcumin (CCM), vemurafenib (VEM), and doxorubicin (DOX), respectively (Noronha et al., 2023). Recent research has shown that ultrasound propagation in liquid systems induces a distinctive acoustic cavitation phenomenon that is characterized by the nucleation, growth, and collapse of microbubbles (Liang et al., 2023). The collapse of these bubbles leads to the local release of high amounts of energy, resulting in the formation of liquid jets, rising pressures, and temperature elevations. Ultrasonic-assisted technologies can address these limitations by promoting interfacial mass transfer and molecular assembly behavior. For instance, Siqueira et al. (2024) reported that the encapsulation efficiency of vitamin E microcapsules increased from 73.73% to 94.05% after combining spray-drying with Ultra-Turrax homogenization and ultrasonic treatment. Notably, the final product showed a yield of 53.2%. Similarly, Cao et al. (2025) developed a soybean whey protein–quercetin nanosystem using 400 W ultrasound treatment. Their strategy achieved reduced particle size, increased ζ-potential values, more uniform dispersion, an encapsulation efficiency of 95.63 ± 0.60%, and a notable improvement in bioavailability. Collectively, these studies demonstrate that ultrasonic technology can achieve the efficient encapsulation of active ingredients in nanosystems by strengthening interfacial interactions.

Although hydrophobic modification and ultrasonic technology have been applied to various biopolymers (e.g., alginate, chitosan, proteins) for bioactive delivery (Han et al., 2023, 2024; Hu et al., 2020), research on such delivery systems based on MD remains relatively scarce despite their significant advantages. Modifying MD with hydrophobic octyl chains can result in amphiphilic derivatives that combine the processing advantages of MD with the self-assembly ability of surfactants. Furthermore, fucoxanthin, which is highly hydrophobic and has poor stability, is an ideal model compound for evaluating the effectiveness of delivery systems. Therefore, we hypothesize that octyl-modified MD, particularly when combined with optimized ultrasonic treatment, constitutes a simple, scalable, and high-performance delivery platform for fucoxanthin.

In this study, MD and octanoyl chloride were used as raw materials to synthesize amphiphilic fatty acyl chloride–maltodextrin sodium derivatives with different degrees of substitution (DS) values via an esterification process. These modified derivatives were designed to self-assemble into micellar-like aggregates for the encapsulation of fucoxanthin. The encapsulation efficiency of fucoxanthin by these self-assembled micelle-like aggregates was evaluated both before and after ultrasonic treatment to examine their loading characteristics, structural and morphological features, and overall physicochemical properties. In addition, an *in vitro* simulated gastrointestinal digestion model was employed to assess the effects of these MD derivatives on the controlled release, digestion, and stability of fucoxanthin. This study aimed to develop a delivery system that can efficiently encapsulate and release fucoxanthin.

2. Materials and methods

2.1. Materials

MD (degree of polymerization, DP 5.0–8.0) and pyrene were both purchased from Aladdin Biochemical Technology Co., Ltd (Shanghai, China). Octanoyl chloride and fucoxanthin were obtained from Macklin Biochemical Technology Co., Ltd (Shanghai, China). Deuterium oxide (D_2O) was purchased from Jin'ouxiang Technology and Trade Co., Ltd (Beijing, China). Additionally, absolute ethanol (EtOH) and phosphate-buffered saline (PBS, pH 7.0) were purchased from Xilong Scientific Co., Ltd (Shantou, China). Saliva, Pepsin, lipase, trypsin, and bile salts were obtained from Yuanye Biotechnology Co., Ltd. (Shanghai, China), while hydrochloric acid (HCl), sodium hydroxide (NaOH), and potassium bromide (KBr) were purchased from Kemiou Chemical Reagent Co., Ltd (Tianjin, China).

2.2. Synthesis of maltodextrin derivatives with different degrees of substitution

The preparation of MD derivatives was carried out based on the method reported by Han et al. (2024), with minor modifications. MD (1 g) was dissolved in a sodium hydroxide solution (10 mL, 0.25 M) at 25 °C and stirred at a low speed of 400 rpm for approximately 10 min to achieve complete dissolution of maltodextrin. Subsequently, octanoyl chloride (10, 50, or 100 μL) was added dropwise to the solution, and the reaction was conducted at room temperature for 1 h until no precipitation was observed. The reaction was terminated by the addition of 100 mL of 95% (v/v) ethanol. The resulting mixture was centrifuged at 6790×*g* for 5 min, and the precipitate was collected, washed with 100 mL of 95% (v/v) ethanol for 2–3 times, and then dried in a vacuum drying oven at 45 °C for 6 h. Finally, the solid powder was redissolved in deionized water and dialyzed in a 3000 Da dialysis bag for 48 h. The solid powder obtained after freeze-drying was sequentially named MD-C8-1, MD-C8-2, and MD-C8-3, corresponding to the increasing volumes of added octanoyl chloride and the gradual increase in the DS. This naming convention is consistent with that used for the ^{1}H nuclear magnetic resonance (NMR) calculation results in the following text.

2.3. Preparation of fucoxanthin-loaded micellar-like aggregates

First, 1 mg/mL MD-C8 solution was prepared, to which 0.1 mg/mL

fucoxanthin ethanol solution was added slowly. The mixture was then subjected to sonication at 400 W (alternately with 5 s ON and 5 s OFF) for 20 min using an ultrasonic cell disruptor (XO-1000D, Nanjing, China), with a 5-min interval every 10 min (Cao et al., 2025). Following sonication, the mixture was dialyzed against deionized water (MWCO 3500 Da) for 48 h, followed by lyophilization. The resulting products were named Ultra-MD-C8-1-FX, Ultra-MD-C8-2-FX, and Ultra-MD-C8-3-FX, corresponding to different DS values. For the control group, the MD-C8 derivative was mixed with the fucoxanthin ethanol solution and stirred in a water bath at 45 °C for 24 h. The mixture was then dialyzed (MWCO 3500 Da) against deionized water for 48 h, and lyophilized. These products were named MD-C8-1-FX, MD-C8-2-FX, and MD-C8-3-FX, also based on their DS values.

2.4. Characterization of hydrophobically modified maltodextrin

2.4.1. ^1H nuclear magnetic resonance (NMR) spectroscopy

The structural analysis of MD-C8 was performed using a 500 MHz NMR spectrometer (Agilent-Varian Mercury Plus 400), as described in our previous study (Han et al., 2024). Samples were dissolved in D_2O, and spectra were recorded at room temperature. The degrees of substitution (DS) were obtained by calculating the ratio between the peak area at 0.8 ppm (three protons of the terminal methyl group of the acyl chloride) and the protons on the MD sugar ring (Zhao et al., 2018). The specific calculation formulas are as follows:

$$DS = \frac{I_{0.8}}{3\left(I_{\alpha-1,6} + I_{\alpha-1,4} + I_{r-e}\right)} \times 100\% \quad (1)$$

where $I_{r\text{-}e}$ corresponds to the ^1H NMR integral of the reducing chainends (α reducing-end signals at 4.95 ppm), $I_{\alpha\text{-}1,4}$ and $I_{\alpha\text{-}1,6}$ are the ^1H NMR integrals of internal α (1 → 4) and α (1 → 6) linkages, Here $I_{\alpha\text{-}1,4}$ and $I_{\alpha\text{-}1,6}$ are the ^1H NMR integrals of internal (1 → 4)- α peaks at approximately 5.21 ppm and (1 → 6)- α linkages around 4.64 ppm, respectively.

2.4.2. Fourier-transform infrared (FTIR) spectroscopy

MD-C8 samples with different DS values were dried in an oven at 40 °C overnight. As described by Han et al. (2024), 1 mg of each dried sample was finely ground with 100 mg of potassium bromide (KBr) and pressed into thin pellets using a manual mold and hydraulic press. The absorption spectra were recorded using an IR Affinity-1 FTIR spectrometer (Shimadzu, Japan) over the wavenumber range of 400-4000 cm^{-1}.

2.4.3. Thermogravimetric analysis (TGA)

The thermal stability of the samples was evaluated using thermogravimetric analysis (SDT 650, TA, USA), following the method reported by Han et al. (2024). First, approximately 4 mg each of MD and MD-C8 samples was placed in a crucible and heated from 30 °C to 600 °C at a rate of 20 °C/min. The relationship between temperature and mass loss was analyzed to assess the thermal stability of the materials.

2.5. Critical aggregation concentration (CAC)

2.5.1. Fluorescence analysis

Pyrene was utilized as a fluorescent probe to determine the CAC via steady-state fluorescence spectroscopy (Han et al., 2024). This technique relies on the linear relationship between surfactant concentration and the fluorescence intensity ratio between peaks I and III (I_1/I_3). MD-C8-pyrene solutions of varying concentrations were prepared in methanol, maintaining a final pyrene concentration of 1×10^{-6} mol/L. Fluorescence spectra were recorded using an FS5 spectrofluorometer (Edinburgh Instruments Ltd., UK).

2.5.2. Dynamic light scattering (DLS)

The CAC was also determined using DLS analysis, following the procedure described in our previous study (Han et al., 2024). MD-C8 solutions of varying concentrations were prepared and filtered through 0.45 μm membranes. Measurements were then performed using a Zetasizer Nano ZS instrument (Malvern Instruments Ltd., UK), and the CAC was calculated based on the inflection point in the plot of hydrodynamic diameter versus concentration.

2.6. Micellar-like aggregate size

The size of micellar-like aggregates produced by MD-C8 in an aqueous solution was determined using a Zetasizer Nano ZS instrument (Malvern Instruments, UK) at 25 °C. Prior to DLS analysis, MD-C8 solutions were filtered through a 0.45 μm microfilter to remove impurities. All measurements were performed in triplicate to ensure data reliability.

2.7. Characterization of fucoxanthin-loaded micellar-like aggregates

Lyophilized MD-C8-FX micelle-like aggregates were dissolved in absolute ethanol to a final concentration of 0.1 mg/mL. After 30 min of ultrasonic treatment (600 W), the mixture was centrifuged at 6800×*g* for 20 min, and the supernatant was collected (Kuang et al., 2024). The concentration of fucoxanthin present in the micelle-like aggregates was quantified by measuring the absorbance at 450 nm using a MAPADA UV-6100 spectrophotometer (China), with reference to an established standard curve (Supplementary data Fig. S1). The encapsulation efficiency (EE) and loading capacity (LC) were calculated using Equations (2) and (3), respectively:

$$EE = \frac{\text{Weight of fucoxanthin in micelle} - \text{like aggregates}}{\text{Weight of Fucoxanthin fed initially}} \times 100\% \quad (2)$$

$$LC = \frac{\text{Weight of Fucoxanthin in micelle} - \text{like aggregates}}{\text{Weight of micelle} - \text{like aggregates containing fucoxanthin}} \times 100\% \quad (3)$$

2.8. Transmission electron microscopy (TEM)

A droplet of the MD-C8 solution was placed on a copper grid. After complete evaporation of the water, background staining was performed using phosphotungstic acid. The micelle-like aggregates size and morphology were then observed using a transmission electron microscope (TEM, JEOL JEM-2100, Japan).

2.9. Environmental stability analysis

Environmental stability of the MD-C8-FX micelle-like aggregates was evaluated using a modified version of the method described by Han et al. (2026). To assess storage stability, fresh samples were stored at room temperature for 2, 4, 6, 10, 14, 21, and 28 days. Samples were taken at each time point, and after ethanol extraction, the concentration of fucoxanthin was determined using an ultraviolet-visible spectrophotometer, with the retention rate calculated according to Equation (4):

$$\text{Retention rate} = \frac{C}{C_0} \times 100\% \quad (4)$$

where C_0 and C represent the initial concentration and the concentration after storage of fucoxanthin, respectively.

The degradation kinetics of fucoxanthin were calculated according to the method reported by (Shang et al., 2023). The degradation rate constant (k) and half-life ($t_{1/2}$) of fucoxanthin were determined from the following equations:

$$\ln\left(\frac{C}{C_0}\right) = -kt \quad (5)$$

$$t_{\frac{1}{2}} = \frac{\ln 2}{k} \quad (6)$$

where C_0 and C represent the initial concentration and the concentration after storage of fucoxanthin, respectively.

To examine photostability, samples were exposed to ultraviolet (UV) light for 30, 60, 90, 120, 150, and 180 min, and the changes in fucoxanthin retention were assessed. To evaluate thermal stability, samples were incubated in a water bath at 25 °C, 37 °C, 50 °C, 65 °C (pasteurization), 80 °C, and 100 °C (boiling/sterilization) for 30 min. To determine humidity stability, samples were exposed to an environment saturated with potassium bromide (RH = 84%) for 2, 4, 6, 8, 10, 12, and 14 days. The retention rate of fucoxanthin was calculated according to the method described in Equation (4).

2.10. In vitro digestion

A simulated oral and gastrointestinal model was employed to investigate the *in vitro* digestion process of MD-C8 micelle-like aggregates, following a modified version of the protocol described by Song et al. (2023). Simulated gastric fluid (SGF) was prepared by dissolving 60 mg NaCl and 96 mg pepsin in 30 mL of 0.1 mol/L PBS buffer. Meanwhile, to prepare simulated intestinal fluid (SIF), 656 mg NaCl, 82.98 mg $CaCl_2$, 120 mg porcine lipase, 120 mg porcine trypsin, and 378 mg bovine bile were dissolved in 20 mL of 0.1 mol/L PBS buffer. All samples, saliva, SGF and SIF were pre-heated to 37 °C before the experiment.

A 20 mg sample of fucoxanthin-loaded micelle-like aggregates were mixed with 5 mL of saliva and stirred at 37 °C for 5 min. The remaining digestion fluid was dispersed in 30 mL of SGF, and the pH was adjusted to 2.0. The mixture was stirred at 37 °C for 2 h. Subsequently, the remaining gastric digest was incubated in a water bath at 37 °C. Then, 20 mL of preheated SIF was added, and the pH was adjusted to 7.0. The system was stirred at 37 °C for 2 h. During this process, 3 mL aliquots were taken at predetermined time points and centrifuged at 6790×*g* for 5 min. The absorbance of the supernatant was measured at 450 nm to calculate the real-time release rate. After the intestinal digestion step, the final round of centrifugation was performed at 6790×*g* for 10 min to isolate the micellar-like aggregates phase. The absorbance of the supernatants was measured at 450 nm, and fucoxanthin concentrations were calculated using a standard calibration curve. The micellization rate and bioaccessibility of fucoxanthin were determined using Equations (7) and (8), respectively.

$$\text{Micellization rate} = \frac{\text{Fucoxanthin content in the micelle phase}}{\text{Fucoxanthin content in the intestinal termination fluid}} \times 100\% \quad (7)$$

$$\text{Bioaccessibility} = \frac{\text{Fucoxanthin content in the micelle phase}}{\text{Fucoxanthin content before simulated gastrointestinal digestion}} \times 100\% \quad (8)$$

2.11. Statistical analysis

All experimental data are presented as the mean ± standard deviation (mean ± SD). Intergroup comparisons were conducted using one-way analysis of variance (one-way ANOVA) via SPSS 26.0 statistical software, with the significance level set at $p < 0.05$ (i.e., *p*-values less than 0.05 were considered statistically significant).

3. Results and discussion

3.1. Synthesis and analysis of maltodextrin derivatives

Fig. 1a shows the ^{1}H NMR spectra of unmodified MD and MD-C8. The characteristic peaks in the 3.0-4.0 ppm and 5.39 ppm regions were attributed to the similar protons of the sugar rings and the anomeric protons of MD (Salehpour et al., 2023). The peak observed at 4.79 ppm was ascribed to the residual, non-deuterated water in D_2O. The absorption peaks of octanoyl chloride protons were observed at 0.8, 1.25, 1.59, and 2.35 ppm, corresponding to the protons on the methyl and methylene groups, respectively. Compared with unmodified MD, all MD-C8 samples showed ^{1}H NMR spectra containing the characteristic absorption peaks from octanoyl chloride protons. These findings confirmed that octanoyl chloride was successfully grafted onto MD (Han et al., 2024). The calculation results also revealed (Table 1) that shown as the average number of substitutes per monomer unit were 0.03 ± 0.003, 0.05 ± 0.006, and 0.07 ± 0.008 in MD-C8-1, MD-C8-2, and MD-C8-3, respectively.

FTIR spectra were employed to assess the structural changes in MD derivatives (Fig. 1b). A broad band was detected at 3318 cm^{-1}, which was attributed to hydrogen-bonded hydroxyl groups. It corresponded to the complex vibrational stretching associated with free, intermolecular, and intramolecularly bound hydroxyl groups that constituted the gross structure of MD. The band at approximately 1645 cm^{-1} was a feature of the tightly bound water present in MD, while that at 2900 cm^{-1} was associated with C-H stretching (Wu et al., 2018). Nevertheless, in the FTIR spectrum of MD-C8, a new peak was observed at 1739 cm^{-1} due to the stretching vibration of the C=O group. This indicated that hydrophobic carbon chains had successfully been grafted onto MD via ester bonds (C=O), confirming the synthesis of the amphiphilic target molecule (Li et al., 2022).

Subsequently, thermal stability was evaluated using the first-order derivatives of weight loss (DTG) and TGA. The TGA results are illustrated in Fig. 1c. Notably, the thermal degradation of MD could be divided into three stages. In the first stage (50-150 °C), the TGA curve revealed slow and continuous mass loss, which was mainly associated with the thermal volatilization of physically adsorbed water molecules on the surface of MD and was unrelated to the decomposition of MD itself. In the second stage (197-400 °C), the TGA curve revealed a rapid and sharp loss of mass, attributed to the thermal decomposition of MD, which involved chemical bond cleavage, decomposition into small-molecule fragments, and their subsequent volatilization. Thus, this stage represented the main decomposition phase of MD. In the third and final stage (400-600 °C), the TGA curve first showed a slow mass loss before finally leveling off. The degradation process of MD during this stage was similar to that of native starch (Wu et al., 2018). Notably, the temperature corresponding to mass loss was found to decrease as the DS increased. Generally, higher decomposition temperatures indicate better thermal stability. Moreover, when alkyl chains are introduced, the thermodynamic stability of MD-C8 tends to decrease (Han et al., 2024). Collectively, the results of this study showed that the decrease in the thermal stability of MD-C8 can be attributed to the weakening of intermolecular forces and hydrogen bonds of MD molecules by the introduction of alkyl chains. These findings provided indirect evidence

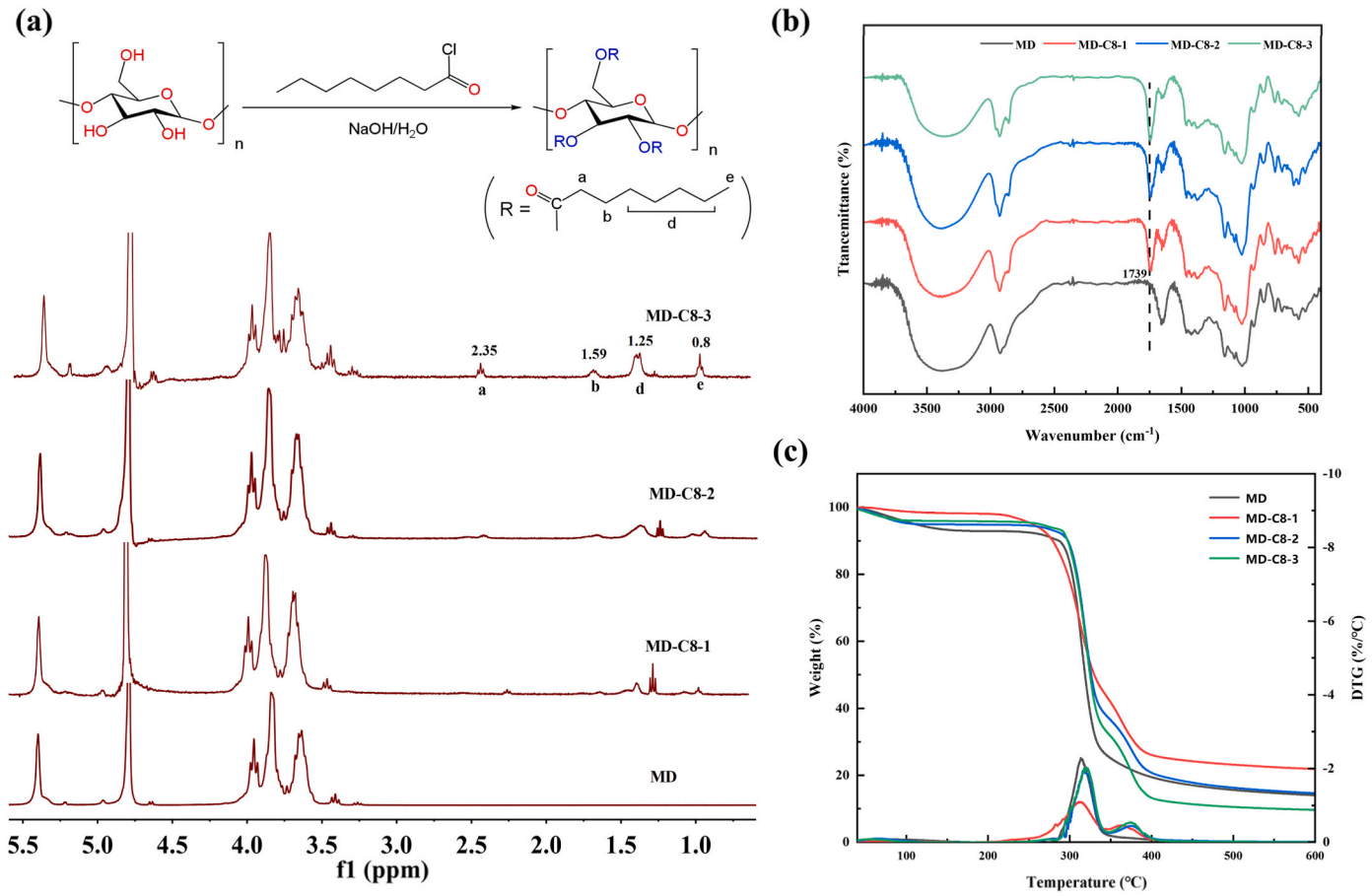

Fig. 1. Structural characterization of maltodextrin and MD-C8: (a) ^{1}H NMR spectra; (b) FTIR spectra; (c) TGA and DTG curves.

Table 1
Properties of different MD-C8 micelle-like aggregate.

Sample	DS	CAC (mg/mL) Fluorescence measurement	CAC (mg/mL) DLS analysis	Hydrodynamic diameters (nm)
MD-C8-1	0.03 ± 0.003^{c}	0.010 ± 0.001^{c}	0.011 ± 0.005^{c}	309.37 ± 1.17^{a}
MD-C8-2	0.05 ± 0.006^{b}	0.005 ± 0.002^{b}	0.005 ± 0.001^{b}	303.72 ± 0.34^{b}
MD-C8-3	0.07 ± 0.008^{a}	0.001 ± 0.001^{a}	0.002 ± 0.002^{a}	279.85 ± 0.97^{c}

Annotation: Different lowercase letters represent the significant differences ($p < 0.05$).

confirming that octanoyl chloride was successfully grafted onto MD via esterification reactions.

3.2. Self-assembly of micellar-like aggregates

The fluorescence emission spectra of MD-C8 polymers in the presence of pyrene are shown in Fig. 2a–c. The changes in fluorescence intensity and peak shape at different MD-C8 concentrations demonstrated that the fluorescence intensity increased significantly as the polymer concentration rose. This indicated that the interaction between the polymer and pyrene was progressively enhanced, reflecting the gradual formation of micellar-like aggregates (Zhao et al., 2022). The difference in fluorescence intensity between the first peak (I_1) and third peak (I_3) also gradually decreased with micelle-like aggregates formation. As shown in Fig. 2d, at low concentrations, the value of I_1/I_3 was 1.80, similar to that of pure water, indicating that no micellar-like aggregates were formed. With the increase in sample concentration, micellar-like aggregates structures began to form gradually. Their hydrophobic cavities could bind to pyrene, resulting in enhanced fluorescence intensity and a gradual decrease in the I_1/I_3 value. The sample concentration corresponding to the inflection point where the I_1/I_3 value began to decrease was defined as the CAC. Accordingly, the CACs of MD-C8-1, MD-C8-2, and MD-C8-3 were calculated to be 0.010 ± 0.001, 0.005 ± 0.002, and 0.001 ± 0.001 mg/mL, respectively (Table 1). The results indicated that with the increase in the DS, more octanoyl chloride molecules are grafted onto MD chains. As a result, hydrophobic interactions are enhanced, thereby promoting micellar-like aggregates formation (Han et al., 2026). Thus, a higher DS promotes the formation of hydrophobic microdomains, which in turn lowers the CAC (Cai et al., 2022).

Fig. 2e shows the relationship between the particle size of MD-C8 samples with different DS values and the sample concentration. Notably, the particle size of the polymer increased with the rise in the sample concentration. However, beyond a specific concentration, the particle size no longer increased and remained stable. This concentration was considered the CAC. Based on this calculation, the CACs of MD-C8-1, MD-C8-2, and MD-C8-3 were found to be 0.011 ± 0.005, 0.005 ± 0.001, and 0.002 ± 0.002 mg/mL, respectively (Table 1). In aqueous solutions, micellar-like aggregates particles are formed by the self-assembly of polar polymers. When the concentration of the polymers is below the CAC, they remain dispersed in aqueous solutions in the form of individual, single polymer chains (Han et al., 2022). However, when their concentration approaches the CAC, these chains aggregate, leading to an increase in the hydrated diameter. As shown in Table 1, the particle sizes of MD-C8-1, MD-C8-2, and MD-C8-3 micelle-like aggregates eventually stabilized at 309.37 ± 1.17, 303.72 ± 0.34, and 279.85 ±

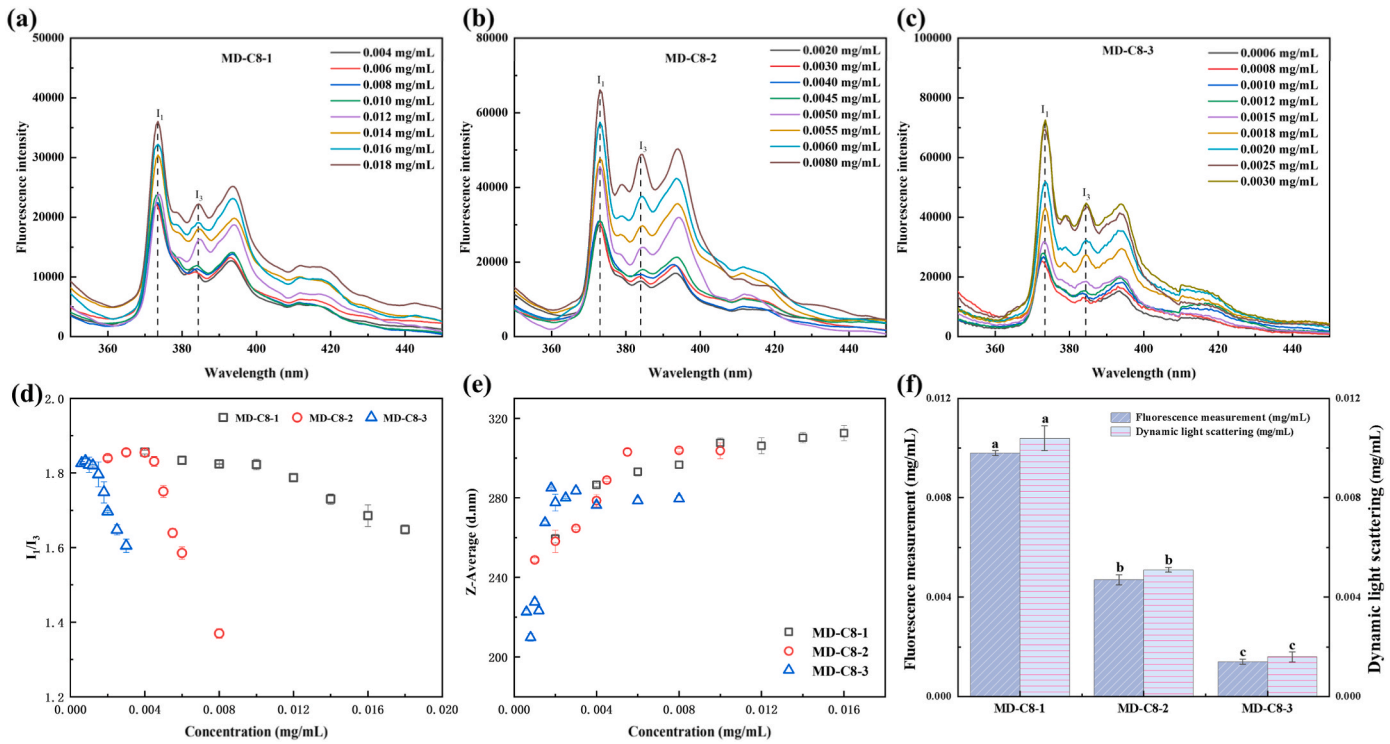

Fig. 2. (a-c) Pyrene fluorescence scanning images of MD-C8 at different concentration levels; (d) Relationship between MD-C8 concentration (different DS values) and the pyrene excitation intensity ratio (I_1/I_3) in aqueous solutions; (e) Hydrated diameter of MD-C8 samples (with different DS values) as a function of concentration; (f) Analysis of the differences between the two CAC determination methods.

Table 2
Properties of different MD-C8-FX micelle-like aggregates.

Micelle Sample	EE (%)	LC (%)	Hydrodynamic Diameters (nm)	Zeta potential (mV)
MD-C8-1-FX	32.53 ± 0.25^{f}	1.60 ± 0.06^{f}	317.23 ± 2.86^{a}	−14.12 ± 0.29^{a}
MD-C8-2-FX	45.06 ± 0.12^{e}	1.79 ± 0.18^{e}	311.80 ± 3.76^{ab}	−13.72 ± 0.74^{a}
MD-C8-3-FX	57.50 ± 0.68^{d}	2.15 ± 0.26^{d}	309.31 ± 4.97^{ab}	−16.03 ± 0.58^{a}
Ultra-MD-C8-1-FX	65.45 ± 0.94^{c}	2.40 ± 0.45^{c}	306.40 ± 5.10^{ab}	−16.03 ± 2.13^{a}
Ultra-MD-C8-2-FX	75.34 ± 1.08^{b}	2.65 ± 0.21^{b}	299.53 ± 2.95^{ab}	−13.83 ± 0.42^{a}
Ultra-MD-C8-3-FX	96.25 ± 1.57^{a}	2.81 ± 0.36^{a}	293.33 ± 4.85^{b}	−16.94 ± 1.30^{a}

Annotation: Different lowercase letters represent significant differences ($p < 0.05$).

0.97 nm, respectively. Fig. 2f shows the comparison of the results obtained via the fluorescence measurement and dynamic light scattering methods, which showed no significant difference ($p < 0.05$). This further verified the accuracy and reliability of the data.

Table 2 lists the EE and the LC values of various MD-C8 samples. The EE values of MD-C8-1-FX, MD-C8-2-FX, and MD-C8-3-FX were 32.53 ± 0.25%, 45.06 ± 0.12%, and 57.50 ± 0.68%, respectively, with corresponding LC values of 1.60 ± 0.06%, 1.79 ± 0.18%, and 2.15 ± 0.26%. Thus, both EE and LC of the micellar-like aggregates evidently rose with the increase in the DS of the polymer derivative. This was because the increase in DS was associated with the enhancement of hydrophobic interactions, which allowed hydrophobic functional groups to bind tightly to the hydrophobic regions within the micelle-like aggregates, thereby increasing the EE and LC values (Han et al., 2024). This was also reflected in the particle size distributions of the micellar-like aggregates. The particle sizes of MD-C8-1-FX, MD-C8-2-FX, and MD-C8-3-FX were 317.23 ± 2.86, 311.80 ± 3.76, 309.31 ± 4.97 nm, respectively. Thus, as the DS increased, the hydrophobic core of the micelle-like aggregates became more tightly bound, leading to a gradual decrease in particle size (Ma et al., 2023; Xie et al., 2024). This result was consistent with our previous reports (Han et al., 2026).

Interestingly, after ultrasonic treatment, both the EE and LC values of the micellar-like aggregates increased significantly, with the EE reaching 65.45 ± 0.94%, 75.34 ± 1.08%, and 96.25 ± 1.57% and the LC reaching 2.40 ± 0.45%, 2.65 ± 0.21%, and 2.81 ± 0.36%, respectively. This significant enhancement can be attributed to the acoustic cavitation effect induced by ultrasound. When ultrasound propagates through the liquid medium, it generates an oscillating pressure field, triggering microbubble nucleation, growth, and violent collapse (transient cavitation) (Ashokkumar, 2011; Chemat et al., 2017). The concentrated energy released by the implosion of these bubbles creates extreme local conditions, accompanied by physical phenomena such as microjet impact and intense shear forces (Ojha et al., 2020). These forces promote the encapsulation of fucoxanthin within MD-C8 micellar-like aggregates through multiple synergistic mechanisms. High shear forces and microjets generated during cavitation can disrupt pre-existing aggregates of both MD-C8 and fucoxanthin, leading to a reduction in particle size (Table 2) and an increase in the available interfacial area for interaction. Simultaneously, the mechanical energy input induces transient unfolding of the polysaccharide chains, thereby exposing hydrophobic pockets that were previously buried and improving the accessibility of fucoxanthin-binding sites. This process also enhances micro mixing within the system, which facilitates the collision and subsequent interaction between hydrophobic fucoxanthin molecules and the exposed hydrophobic domains of MD-C8, effectively

overcoming diffusion limitations. Furthermore, the transient local high temperatures generated during bubble collapse increase the mobility of polymer chains and solute molecules, thereby reinforcing the thermodynamic driving force for hydrophobic interactions and promoting the incorporation of fucoxanthin into the micellar core (Cai et al., 2022).

The comparison table between MD-C8-3-FX (EE 57.50%) and Ultra-MD-C8-1-FX (EE 65.45 ± 0.94%) shows that after 20 min of ultrasonic treatment, even the micellar-like aggregates with low DS have higher drug loading capacity than those with high DS but without ultrasonic treatment. However, the hydrophobic domains of hydrophobically modified MD are usually encapsulated in the micellar-like aggregates structure, resulting in relatively low binding with fucoxanthin. Notably, the shockwaves generated by ultrasonic treatment can reduce intermolecular forces and hydrogen bond formation. Ultimately, as the MD chain unfolds, hydrophobic groups previously hidden within the micellar-like aggregates structure are exposed to the external environment, significantly strengthening the interaction with fucoxanthin (Cao et al., 2025). Moreover, briefly optimized ultrasonic treatment can dynamically enhance the encapsulation capacity of the system through the aforementioned mechanisms, compensating for the low degree of substitution. However, it should be noted that excessive ultrasonic energy or duration may degrade sensitive bioactive compounds and damage polymer integrity (Wang et al., 2023). Therefore, the parameters adopted in this study were optimized to maximize beneficial effects (see Supplementary data Fig. S2.) while minimizing any adverse impacts. This indicates that ultrasonic treatment can overcome the drug loading limitations associated with low DS and effectively promote the hydrophobic aggregation of MD molecules. Meanwhile, when compared with those of other carriers for fucoxanthin encapsulation, the EE value of the Ultra-MD-C8-3-FX (96.3%) was higher than that of fucoxanthin loaded in alginate/chitosan nanoparticles (81.2%) (Sorasitthiyanukarn et al., 2024). The performance of the MD-C8 micellar system also outperformed starch/zein-based microcapsules (EE 91%) (Zhao et al., 2022). The improvement of this drug loading capacity helps reduce the loss of fucoxanthin, improve the efficacy of fucoxanthin, and lower the preparation cost of fucoxanthin-loaded micellar-like aggregates.

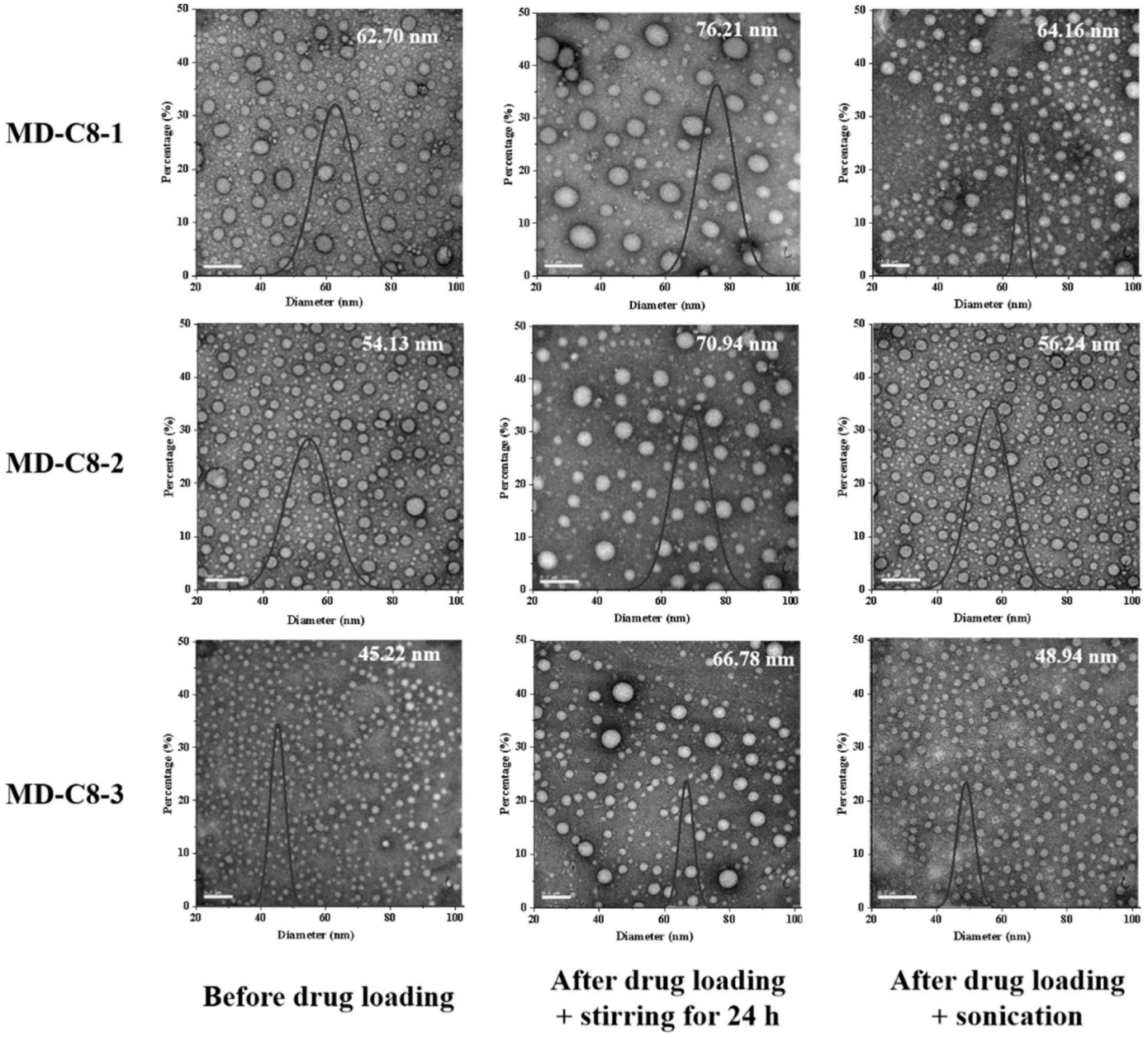

Fig. 3. TEM images showing the morphologies of MD-C8-1, MD-C8-2, and MD-C8-3 micelle-like aggregates before and after fucoxanthin loading. Scale bar: 200 nm.

In this study, subsequent to ultrasonic treatment, the particle sizes of Ultra-MD-C8-1-FX, Ultra-MD-C8-2-FX, and Ultra-MD-C8-3-FX decreased to 306.40 ± 5.10, 299.53 ± 2.95, and 293.33 ± 4.85 nm, respectively (Table 2). This finding implies that ultrasonic treatment has the potential to reduce the particle size of micellar-like aggregates and facilitate their hydrophobic aggregation (Yang et al., 2020). Following the stirring treatment, the zeta potentials of MD-C8-1-FX, MD-C8-2-FX, and MD-C8-3-FX were measured to be −14.12 ± 0.29, −13.72 ± 0.74, and −16.03 ± 0.58 mV, respectively (Table 2). Subsequently, after the ultrasonic treatment, the corresponding zeta potential values for Ultra-MD-C8-1-FX, Ultra-MD-C8-2-FX, and Ultra-MD-C8-3-FX altered to −16.03 ± 2.13, −13.83 ± 0.42, and −16.94 ± 1.30 mV, respectively (Table 2). There was no significant difference in the zeta potential of the micellar-like aggregates before and after sonication ($p > 0.05$, Table 2), which indicates that sonication had a negligible effect on the zeta potential of MD micellar-like aggregates, indicating that the ultrasound treatment did not alter the fundamental surface charge characteristics of the MD-C8 derivatives, but primarily affected their physical assembly and loading dynamics. However, the relatively low absolute zeta potential values of MD-C8 micellar-like aggregates (ranging from −13 to −17 mV, Table 2) indicate a moderate electrostatic repulsion between micellar-like aggregates. Higher values within the range of ±30 mV indicate stable dispersions, whereas a value closer to zero implies less stability and may induce aggregation (Agmo Hernández, 2023; Rodriguez-Loya et al., 2024). Hence, such repulsion may be insufficient to completely prevent their close contact and transient association in the solution, thereby facilitating the formation of larger, reversible clusters that dominate the DLS signal. This also offers a straightforward rationale for the large hydrated particle size of MD-C8 micellar-like aggregates detected in the DLS measurements.

As shown in Fig. 3, no significant changes in micellar-like aggregates morphology were observed before and after fucoxanthin loading. Notably, both MD-C8 and MD-C8-FX micelle-like aggregates appeared spherical or ellipsoidal in shape. However, the particle size of the micelle-like aggregates was found to be significantly altered after fucoxanthin loading. Before drug loading, the particle size of the micellar-like aggregates was relatively small, with MD-C8-1, MD-C8-2, and MD-C8-3 showing particle sizes of 62.70, 54.13, and 45.22 nm, respectively. Moreover, these micellar-like aggregates were observed to be well-dispersed. After drug loading through 24 h of stirring, the particle sizes of the micellar-like aggregates became slightly greater than those of the blank micellar-like aggregates, reaching 76.21, 70.94, and 66.78 nm, respectively. This was attributed to the incorporation of fucoxanthin into the core of the micellar-like aggregates, which increased the region of hydrophobicity and thus increased the particle size (Han et al., 2024). After ultrasonic-assisted drug loading, the particle sizes of the micellar-like aggregates were found to be 64.16, 56.24, and 48.94 nm, respectively. Thus, the sizes of these particles were higher than those of the blank micelle-like aggregates but lower than those of the drug-loaded micellar-like aggregates prepared through stirring. The findings indicated that ultrasonic treatment for an appropriate duration may induce structural relaxation in MD-C8, thus increasing the exposure of hidden moieties and promoting intermolecular electrostatic repulsion and hydrophobic interactions (Liang et al., 2023). Thus, the cavitation effect generated by ultrasound can reduce the particle size of micellar-like aggregates and promote the formation of a more compact hydrophobic core. In addition, we found that with the increase in DS, the particle sizes of the micellar-like aggregates decreased gradually, and the dispersibility of the particles improved. These results were consistent with the DLS results (Tables 1 and 2), although the particle sizes measured by TEM were smaller than those determined using DLS. This difference was mainly attributed to the variations in the sample preparation process. Specifically, the particle size measured by TEM corresponded to the size of the micelle-like aggregates in a dry state, while that measured by DLS represented the hydrodynamic diameter of the micellar-like aggregates (Li et al., 2022). DLS is an intensity-weighted technique for measuring hydrodynamic diameter. Therefore, a small number of secondary micellar-like aggregates or clusters formed by weak intermolecular interactions between micelles in the solution can significantly overestimate the measured results (Qiao et al., 2015). While TEM offers a number-weighted visualization of samples in a dried and fixed state, the drying and staining steps during sample preparation not only disrupt such weak noncovalent clusters but also lead to the shrinkage of flexible polysaccharide coronas and the loss of hydration shells, thereby only revealing the dense core structure of individual micelles. As described the zeta potential values of MD-C8 micellar-like aggregates (ranging from −13 to −17 mV, Table 2) were relatively low. The electric double layer is compressed due to insufficient charge, and the electrostatic repulsion barrier is greatly reduced, which cannot fully counteract the van der Waals forces between particles. As a result, micellar-like aggregates tend to form loose secondary aggregates/clusters through weak interactions such as hydrophobic effects, hydrogen bonding and van der Waals forces (Bhattacharjee, 2016). Therefore, the actual particle size measured by DLS corresponds to that of the agglomerated secondary aggregates or clusters, which results in a significant discrepancy between the DLS and TEM results (Wilson & Prud'homme, 2021). Moreover, due to the solvent effect under hydrated conditions, the micellar-like aggregates were observed to possess a larger hydrodynamic volume.

3.3. Environmental stability analysis

Although the structural characteristics of MD-C8 provided some insights into its potential activity, a comprehensive evaluation of its real-life performance was still needed. Fig. 4a illustrates the storage stability of free and MD-C8-encapsulated fucoxanthin. As the storage time was prolonged, fucoxanthin underwent varying degrees of photodegradation, and its retention rate decreased accordingly. After 28 days of storage, the retention rates of fucoxanthin in MD-C8-1-FX, MD-C8-2-FX, MD-C8-3-FX, Ultra-MD-C8-1-FX, Ultra-MD-C8-2-FX, and Ultra-MD-C8-3-FX were found to be 49.16%, 52.22%, 54.25%, 57.37%, 60.29%, and 62.01%, respectively. The retention rates of encapsulated fucoxanthin were over 50% in almost all samples, while the retention rate of free fucoxanthin was significantly lower at 44.56%. This indicated that modified MD can effectively protect fucoxanthin and reduce its light-induced degradation. This protective effect was attributed to the increase in hydrophobic groups on the surface of MD following ultrasound treatment. Ultrasonication likely promoted the interactions between MD-C8 and fucoxanthin, thereby improving the storage stability of fucoxanthin (Cao et al., 2025). Furthermore, the first-order kinetic model was used to describe the degradation behavior of fucoxanthin during storage (Fig. 4e). The half-lives of free fucoxanthin and that encapsulated in MD-C8-1-FX, MD-C8-2-FX, MD-C8-3-FX, Ultra-MD-C8-1-FX, Ultra-MD-C8-2-FX, and Ultra-MD-C8-3-FX micellar-like aggregates were 21.35 d, 24.98 d, 27.35 d, 29.75 d, 32.19 d, 34.35 d and 37.35 d, respectively. With the increase in DS, the half-life of fucoxanthin in the micelle-like aggregates was prolonged; in addition, the micelle-like aggregates after sonication exhibited a more significant prolongation effect on fucoxanthin stability. Therefore, the degradation kinetic model also confirms that the hydrophobically modified maltodextrin aggregates can effectively slow down the degradation rate of fucoxanthin (Shang et al., 2023).

Similarly, when free and encapsulated fucoxanthin were exposed to UV light for 180 min, the retention rates have shown a similar trend to those seen during storage. The retention rates of MD-C8-FX-1, MD-C8-FX-2, MD-C8-FX-3, Ultra-MD-C8-FX-1, Ultra-MD-C8-FX-2 and Ultra-MD-C8-FX-3 were 62.87%, 64.64%, 67.59%, 68.86%, 71.30%, and 74.51% respectively (Fig. 4b). Meanwhile, free fucoxanthin was more significantly affected by UV irradiation, exhibiting a retention rate of only 48.09%. It speculated that the encapsulating micellar-like aggregates structures protected fucoxanthin by reducing its exposure to oxygen and light (Mulrooney et al., 2021). Notably, the retention rates of

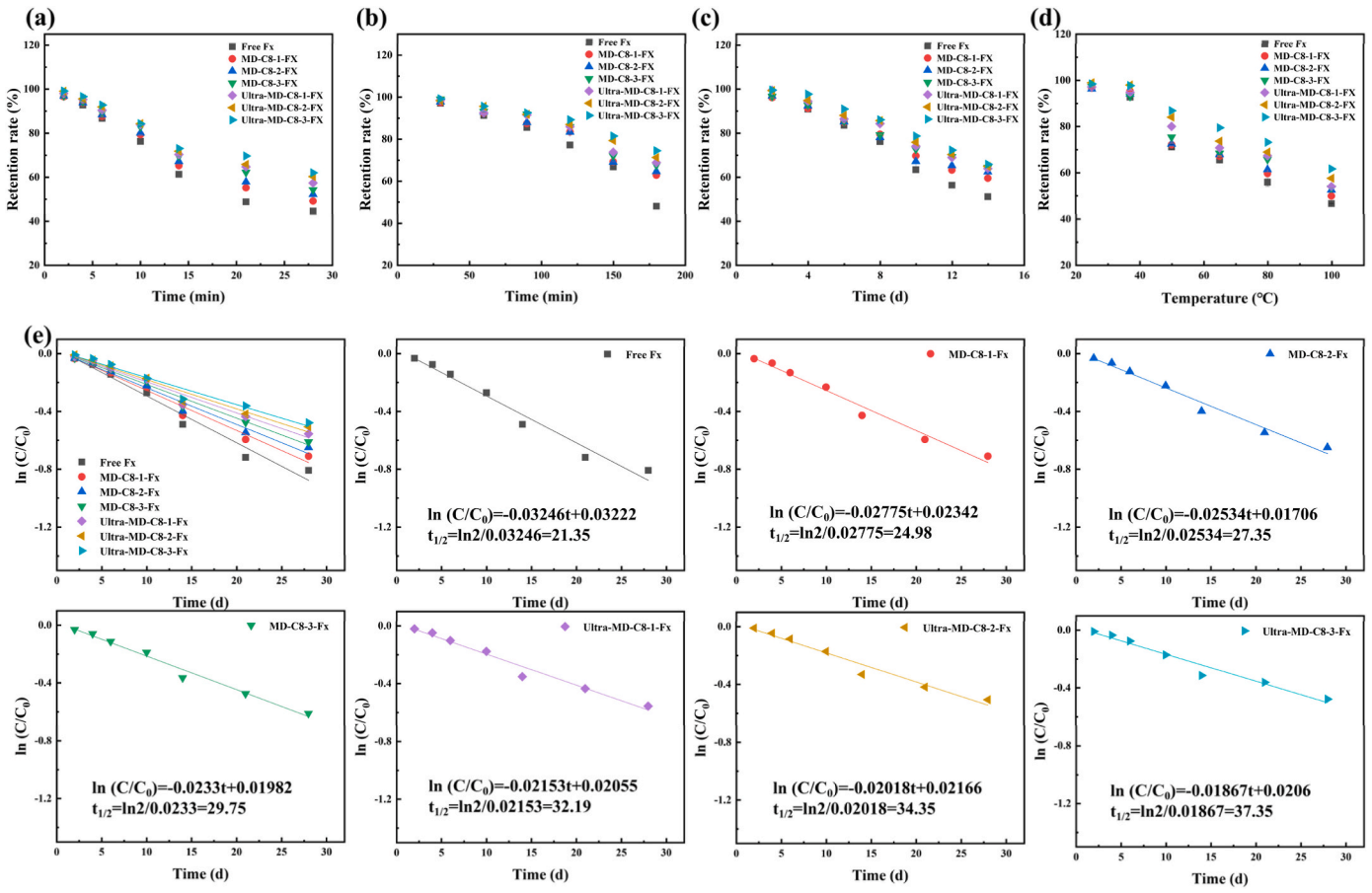

Fig. 4. Storage stability (a), ultraviolet stability (b), humidity stability (c), and thermal stability (d) of MD-C8 micelle-like aggregates.

MD-C8 after ultrasonic treatment were all higher than those seen in the 24 h stirring group, in line with the higher EE and LC values. Since a larger amount of fucoxanthin was encapsulated in ultrasonically treated micelle-like aggregates, despite partial loss of fucoxanthin, the final retention rate remains high.

As shown in Fig. 4c, the samples were also exposed to a closed environment with 85% relative humidity (RH) for 14 days. Following this period, the retention rate of free fucoxanthin dropped to only 51.13%. However, encapsulated fucoxanthin exhibited better stability under conditions of high RH than its free form. the retention rates of MD-C8-1-FX, MD-C8-2-FX, MD-C8-3-FX, Ultra-MD-C8-1-FX, Ultra-MD-C8-2-FX, and Ultra-MD-C8-3-FX, though decreasing significantly, still reached 59.56%, 62.46%, 64.43%, 63.93%, 64.93%, and 65.98% respectively. The encapsulated fucoxanthin was located within the hydrophobic core of the micellar-like aggregates, whose outer shell could shield fucoxanthin from the harsh humid environment and thereby slow down its degradation rate. After ultrasonic treatment, the particle sizes of the micelle-like aggregates decreased considerably, and their binding became tighter. This provided a more favorable environment for the storage of fucoxanthin, as reflected by the higher retention rate.

As shown in Fig. 4d, the thermal stability of free and encapsulated fucoxanthin in MD-C8 particles was evaluated primarily under simulated pasteurization and boiling/sterilization conditions. The retention rate of free fucoxanthin was 65.51% after heating at 65 °C for 30 min, while the retention rates of the fucoxanthin encapsulated in MD-C8-1-FX, MD-C8-2-FX, MD-C8-3-FX, Ultra-MD-C8-1-FX, Ultra-MD-C8-2-FX, and Ultra-MD-C8-3-FX were significantly higher (67.23%, 67.94%, 68.47%, 70.79%, 73.69%, and 79.49%, respectively). A similar trend was observed after the samples were heated at 100 °C for 30 min, with free fucoxanthin, MD-C8-1-FX, MD-C8-2-FX, MD-C8-3-FX, Ultra-MD-C8-1-FX, Ultra-MD-C8-2-FX, and Ultra-MD-C8-3-FX showing retention rates of 46.67%, 49.94%, 52.59%, 53.43%, 54.04%, 57.64%, and 61.72% respectively. During commercial applications, especially in liquid products, thermal sterilization is often performed to prevent microbial contamination. However, high-temperature treatment can lead to the degradation of fucoxanthin. Our findings showed that although heat treatment can partly disrupt the structure of modified MD micellar-like aggregates, thereby accelerating fucoxanthin degradation, the hydrophobic core of these micelle-like aggregates can effectively protect fucoxanthin, thus mitigating the impact of thermal stress. Notably, the retention rate after heating remained higher in the ultrasonic treatment group than in the 24-h stirring group. This suggested that appropriate ultrasonic treatment can significantly enhance the thermal stability of fucoxanthin in a hydrophobically modified MD-based composite system (Cao et al., 2025).

3.4. Fucoxanthin release from micelle-like aggregates in vitro

Fig. 5 shows the fucoxanthin release rate curves of MD-C8-FX at different time points during *in vitro* digestion (Fig. 5a). As reported previously (Han et al., 2024), the release rate of free fucoxanthin was below 5% after simulated digestion. This indicated that free fucoxanthin was not susceptible to the simulated oral and gastrointestinal digestion and showed limited dispersion in the digestive fluids. The cumulative release rate of MD-C8 micelle-like aggregates following brief salivary digestion was below 10%. Maltodextrin is a hydrolysis product of starch and can be digested by salivary amylase in the oral cavity. Due to the short residence time and near-neutral pH in the oral phase, the MD-C8 micelle-like aggregates remained intact, with only a slight release of fucoxanthin. However, under simulated gastric conditions, throughout

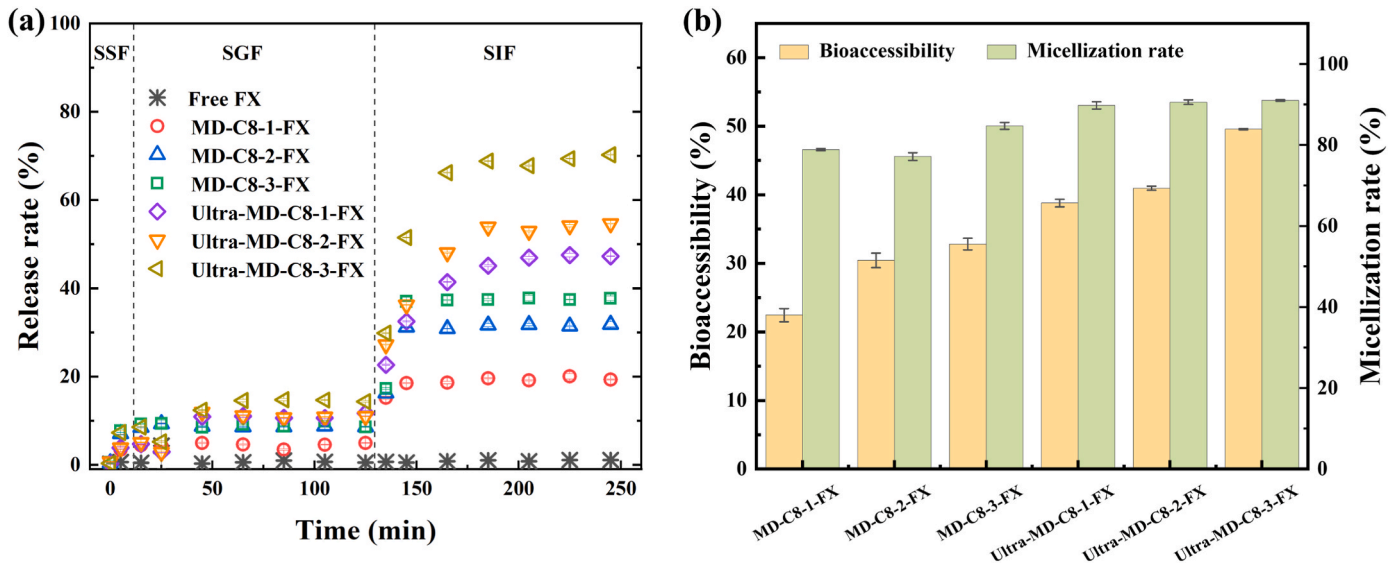

Fig. 5. (a) Time-dependent cumulative release of free fucoxanthin and fucoxanthin loaded within micelle-like aggregates in simulated gastric and intestinal environments, monitored based on absorbance at 450 nm; (b) Bioaccessibility and micellization rate of MD-C8-loaded fucoxanthin in an *in vitro* simulated digestion model.

the 120-min gastric digestion phase, and the release rate in the stomach was consistently below 15%. This indicated only minimal release of fucoxanthin during gastric digestion, which was likely derived from the fucoxanthin that was either loosely adsorbed onto the surface of the MD-C8 micelles or trapped near the micellar-like aggregates interface (Liu et al., 2024), while the majority of encapsulated fucoxanthin was retained within the micellar-like aggregates core (Ahmad et al., 2019). The strong hydrophobic interactions between fucoxanthin and MD-C8 create a micelle-like aggregates structure where the hydrophilic regions are exposed to the exterior, creating a dense hydrophilic shell that provides protection in the acidic gastric environment and prevents the premature release of fucoxanthin (Li et al., 2024).

In contrast, in the small intestinal phase, the micellar-like aggregates began to release fucoxanthin in large quantities. After 10 min of digestion in the SIF, a significant increase in the absorbance of fucoxanthin was observed. These results all indicated that fucoxanthin could be released in large amounts in the small intestine, with the release stabilizing after 40 min. Notably, the absorbance values were in the following ascending order: MD-C8-1-FX < MD-C8-2-FX < MD-C8-3-FX < Ultra-MD-C8-1-FX < Ultra-MD-C8-2-FX < Ultra-MD-C8-3-FX, and the release rate of Ultra-MD-C8-3-FX at the end of small intestinal digestion reached up to 70.26 ± 0.07%. Micelles prepared via 20 min of ultrasonic treatment released more fucoxanthin than those prepared by stirring for 24 h. This difference was positively correlated with the drug-loading capacity of the micelle-like aggregates, with higher loading capacity resulting in greater release in the intestine. While starch/zein-based microcapsules for encapsulation and delivery of fucoxanthin exhibited intestinal segmental controlled release with a relatively lower *in vitro* release rate of 42% (Zhao et al., 2022). These findings further confirmed that ultrasonic treatment enhances the fucoxanthin-loading capacity of hydrophobically modified MD (MD-C8) derivatives.

The bioaccessibility of fucoxanthin was also evaluated using an *in vitro* digestion model, as shown in Fig. 5b. The bioaccessibility values for MD-C8-1-FX, MD-C8-2-FX, MD-C8-3-FX, Ultra-MD-C8-1-FX, Ultra-MD-C8-2-FX, and Ultra-MD-C8-3-FX were 22.45%, 30.43%, 32.81%, 38.79%, 40.96%, and 49.57%, respectively. As the DS increased, the bioaccessibility of fucoxanthin also improved. Furthermore, samples treated with ultrasound exhibited significantly enhanced bioaccessibility. Moreover, the micellization rates for these samples were 78.86%, 77.14%, 84.7%, 89.75%, 90.54%, and 90.96%, respectively. These results were consistent with the physicochemical properties of fucoxanthin. First, due to its poor water solubility, fucoxanthin requires delivery via carrier materials to reach the small intestine, where it can be absorbed by intestinal epithelial cells (Kuang et al., 2024). Second, micellization is a critical step for enhancing the delivery of hydrophobic compounds (Cheng et al., 2019). Thus, hydrophobically modified MD micellar-like aggregates could facilitate the delivery of fucoxanthin to the absorption sites in the intestine. Specifically, a higher micellization efficiency leads to greater fucoxanthin loading and more effective delivery. Thus, there exists a strong positive correlation between fucoxanthin bioaccessibility and micellization efficiency.

4. Conclusion

In summary, hydrophobically modified MD derivatives with varying DS values were successfully synthesized in this study. A variety of methods were employed to systematically evaluate the structural characteristics and self-assembly behavior of the resulting MD-C8 composites. It was found that MD-C8, with a CAC ranging from 0.002 to 0.011 mg/mL, could self-assemble into spherical micellar-like aggregates with particle sizes between 279.85 ± 0.97 nm and 309.37 ± 1.17 nm. Due to their amphiphilic nature, the synthesized micelle-like aggregates were capable of encapsulating the hydrophobic compound fucoxanthin, particularly following ultrasonic treatment. Among the derivatives, those with higher DS values exhibited superior EE and LC. Moreover, appropriate ultrasound treatment significantly enhanced the EE of the micelle-like aggregates. Subsequently, TEM revealed that ultrasonic treatment, due to the cavitation effect, reduced the particle size of the micelle-like aggregates and promoted their uniform dispersion. Overall, the fucoxanthin encapsulated in hydrophobically modified MD-C8 micelle-like aggregates demonstrated enhanced environmental stability, including improved resistance to storage, UV light, temperature, and humidity, as well as favorable stability during simulated gastrointestinal digestion. Notably, compared with MD-C8-1-FX, the Ultra-MD-C8-3-FX micelle-like aggregates increased the bioaccessibility of fucoxanthin by 2.21-fold, achieving a micellization efficiency of up to 90.96%. This study provides valuable insights into strategies for the efficient delivery of hydrophobic bioactive compounds. Specifically, it indicates that MD-C8 micelle-like aggregates demonstrate strong potential as delivery carriers, and ultrasound is an effective auxiliary strategy to improve the encapsulation performance of these micelle-like aggregates. The existing MD is derived from low-cost polysaccharides widely used in food.

Through relatively simple modification combined with a rapid ultrasound-assisted loading process, it achieves a convincing balance between high performance, simplicity, and economic feasibility. This highlights MD-C8 micelle-like aggregates potential as a practical and efficient delivery strategy for hydrophobic bioactive substances such as fucoxanthin.

CRediT authorship contribution statement

Lingyu Han: Writing – review & editing, Writing – original draft, Methodology, Investigation, Formal analysis. **Mengsi Nong:** Writing – review & editing, Writing – original draft, Methodology, Investigation. **Jixin Yang:** Writing – review & editing, Methodology, Formal analysis, Conceptualization. **Jijuan Cao:** Writing – review & editing, Methodology, Conceptualization. **Bing Hu:** Writing – review & editing, Writing – original draft, Methodology, Conceptualization. **Peter A. Williams:** Writing – review & editing, Methodology, Formal analysis, Conceptualization.

Declaration of competing interest

Professor Peter A. Williams is the Editor-in-Chief of Food Hydrocolloids and consequently the manuscript should be assigned to Professor Fang Zhong who is an Associate editor of the Journal and has the necessary knowledge to undertake the review process.

Acknowledgements

This article was funded by Liaoning Provincial Science and Technology Plan Joint Fund Project (2025JH2/101800265), National Natural Science Foundation of China (No. 32202232), Fundamental Research Funds for the Central Universities (044420250051), and Key research and Development Project of Liaoning Province (2024JH2/102400055).

Appendix A. Supplementary data

Supplementary data to this article can be found online at https://doi.org/10.1016/j.foodhyd.2026.112641.

Data availability

Data will be made available on request.

References

Agmo Hernández, V. (2023). An overview of surface forces and the DLVO theory. *ChemTexts, 9*(4).

Ahmad, M., Mudgil, P., Gani, A., Hamed, F., Masoodi, F. A., & Maqsood, S. (2019). Nano-encapsulation of catechin in starch nanoparticles: Characterization, release behavior and bioactivity retention during simulated in-vitro digestion. *Food Chemistry, 270*, 95–104.

Ashokkumar, M. (2011). The characterization of acoustic cavitation bubbles – An overview. *Ultrasonics Sonochemistry, 18*(4), 864–872.

Bhattacharjee, S. (2016). DLS and zeta potential – What they are and what they are not? *Journal of Controlled Release, 235*, 337–351.

Cai, W., Hu, T., Cai, W., & Huang, Q. (2022). Ultrasound-induced changes in rheological behavior and hydrophobic microdomains of Lignosus rhinocerotis polysaccharide. *International Journal of Biological Macromolecules, 213*, 565–573.

Cao, X., Cao, J., Xu, T., Zheng, L., Dai, J., Zhang, X., Tian, T., Ren, K., Tong, X., Wang, H., & Jiang, L. (2025). Construction of nanodelivery system based on the interaction mechanism between ultrasound–treated soybean whey protein and quercetin: Structure, physicochemical stability and bioaccessibility. *Ultrasonics Sonochemistry, 112*, Article 107195.

Chemat, F., Rombaut, N., Sicaire, A.-G., Meullemiestre, A., Fabiano-Tixier, A.-S., & Abert-Vian, M. (2017). Ultrasound assisted extraction of food and natural products. Mechanisms, techniques, combinations, protocols and applications. A review. *Ultrasonics Sonochemistry, 34*, 540–560.

Cheng, C. J., Ferruzzi, M., & Jones, O. G. (2019). Fate of lutein-containing zein nanoparticles following simulated gastric and intestinal digestion. *Food Hydrocolloids, 87*, 229–236.

Han, L., Sun, J., Williams, P. A., Yang, J., & Zhang, S. (2022). Octenyl-succinylated inulins for the delivery of hydrophobic drug. *International Journal of Biological Macromolecules, 221*, 1112–1120.

Han, L., Zhai, R., Hu, B., Williams, P. A., Yang, J., Zhang, C., Dong, N., & Li, T. (2024). Preparation and characterization of hydrophobically-modified sodium alginate derivatives as carriers for fucoxanthin. *Food Hydrocolloids, 157*, Article 110386.

Han, L., Zhai, R., Hu, B., Yang, J., Li, Y., Xu, Z., Meng, Y., & Li, T. (2023). Effects of octenyl-succinylated chitosan-whey protein isolated on emulsion properties, astaxanthin solubility, stability, and bioaccessibility. *Foods, 12*, 2898.

Han, L., Zhai, R., Williams, P. A., Hu, B., Yang, J., Dong, N., Ban, Y., & Li, T. (2026). Hydrophobic derivatization of sodium alginate for use in fucoxanthin delivery. *Food Hydrocolloids, 170*, Article 111664.

Hu, B., Wang, K., Han, L., Zhou, B., Yang, J., & Li, S. (2020). Pomegranate seed oil stabilized with ovalbumin glycated by inulin: Physicochemical stability and oxidative stability. *Food Hydrocolloids, 102*, Article 105602.

Kim, D., Lee, Y. Y., Kim, H. J., Choi, M., Lee, S., Kim, H. E., Kim, E., Jo, M., & Choi, Y. J. (2025). Enhanced storage and gastrointestinal stability of spray-dried whey protein emulsions with chitosan and gum Arabic. *International Journal of Biological Macromolecules, 299*, Article 140260.

Kuang, H., Ma, L., Guo, Y., & Liu, Y. (2024). Chitosan surface-modified bovine serum albumin-oleic acid self-assembled complexes: Improving the thermal stability, controlled release and bioaccessibility of fucoxanthin. *Food Hydrocolloids, 151*, Article 109796.

Li, H., Hou, Y., Jia, S., Tan, M., & Wang, H. (2024). Oxidized paramylon self-assembled nanoparticles loaded with fucoxanthin attenuate insulin resistance in HpeG2 cells. *Carbohydrate Polymers, 345*, Article 122597.

Li, H., Yang, H., Xu, J., Gao, Z., Wu, J., Zhu, L., & Zhan, X. (2022). Novel amphiphilic carboxymethyl curdlan-based pH responsive micelles for curcumin delivery. *LWT, 153*, Article 112419.

Liang, Q., Zhou, C., Rehman, A., Qayum, A., Liu, Y., & Ren, X. (2023). Improvement of physicochemical properties, microstructure and stability of lotus root starch/xanthan gum stabilized emulsion by multi-frequency power ultrasound. *Ultrasonics Sonochemistry, 101*, Article 106687.

Liu, M., Wang, X., Li, Y., Jin, D., Jiang, Y., Fang, Y., Lin, Q., & Ding, Y. (2024). Effects of OSA-starch-fatty acid interactions on the structural, digestibility and release characteristics of high amylose corn starch. *Food Chemistry, 454*, Article 139742.

Ma, Y., Li, M., Chen, Z., Feng, J., Chen, R., Wang, Z., Chen, J., & Zhang, S. (2023). Construction of butyric acid modified porous starch for stabilizing pickering emulsions: Encapsulation of paclitaxel. *Food Hydrocolloids, 142*, Article 108858.

Mulrooney, S. L., O'Neill, G. J., Brougham, D. F., Lyng, J. G., & O'Riordan, D. (2021). Improving vitamin D3 stability to environmental and processing stresses using mixed micelles. *Food Chemistry, 362*, Article 130114.

Noronha, M. A., D'Angelo, N. A., Pérez-Sánchez, G., Severino, P., Ann Foglio, M., Greaves, T. L., Pereira, J. F. B., & Lopes, A. M. (2023). Self-assembling micelles of lipopolysaccharides (LPS) for loading hydrophobic (bio)molecules. *Journal of Molecular Liquids, 372*, Article 121154.

Ojha, K. S., Aznar, R., O'Donnell, C., & Tiwari, B. K. (2020). Ultrasound technology for the extraction of biologically active molecules from plant, animal and marine sources. *Trends in Analytical Chemistry, 122*, Article 115663.

Qiao, B., Ferru, G., Olvera de la Cruz, M., & Ellis, R. J. (2015). Molecular origins of mesoscale ordering in a metalloamphiphile phase. *ACS Central Science, 1*(9), 493–503.

Rodriguez-Loya, J., Lerma, M., & Gardea-Torresdey, J. L. (2024). Dynamic light scattering and its application to control nanoparticle aggregation in colloidal systems: A review. *Micromachines, 15*, 24.

Sahiner, M., Gungor, B., Silan, C., Demirci, S., Erdogan, H., Ayyala, R. S., & Sahiner, N. (2024). Synthesis and characterization of poly (Maltodextrin) microgel from maltodextrin as drug delivery system. *Reactive and Functional Polymers, 195*, Article 105826.

Salehpour, N., Bayatloo, M. R., & Nojavan, S. (2023). Green hydrophobic maltodextrin nanosponges for magnetic solid-phase extraction of hypothalamic peptides from plasma samples. *Journal of Chromatography A, 1706*, Article 464220.

Shang, W., Sun, Y., Song, J., Zhang, P., Hou, Y., Wang, H., & Tan, M. (2023). Novel high internal phase oleogels-in-water pickering emulsions stabilized solely by whey protein isolate for 3D printing and fucoxanthin delivery. *Food Hydrocolloids, 140*, Article 108609.

Sia, Y. J., Chua, L. S., Aman Nor, N. F., Soo, J., & Sari, E. (2025). Spray drying and characterisation of anthocyanin rich microcapsules from jaboticaba juice with maltodextrin. *Food Bioscience, 68*, Article 106446.

Siqueira, L., Ballus, C. A., Tanabe, E. H., & Bertuol, D. A. (2024). Combining ultra-turrax and ultrasonic homogenization to achieve higher vitamin E encapsulation efficiency in spray drying. *Particuology, 95*, 28–35.

Song, J., Li, H., Shang, W., Wang, H., & Tan, M. (2023). Fabrication and characterization of pickering emulsion gels stabilized by gliadin/starch complex for the delivery of astaxanthin. *Food Hydrocolloids, 137*, Article 108388.

Sorasitthiyanukarn, F. N., Muangnoi, C., Rojsitthisak, P., & Rojsitthisak, P. (2024). Stability and biological activity enhancement of fucoxanthin through encapsulation in alginate/chitosan nanoparticles. *International Journal of Biological Macromolecules, 263*, Article 130264.

Suenaga, R., Komuro, Y., & Terao, K. (2025). Highly soluble and well-defined polysaccharide-based micelle in aqueous media: Decyl succinic anhydride-modified pullulan. *Carbohydrate Polymers, 358*, Article 123504.

Thongpon, P., Intuyod, K., Pongking, T., Priprem, A., Chomwong, S., Tanasuka, P., Mahalapbutr, P., Suriya, U., Vaeteewoottacharn, K., Pinlaor, P., & Pinlaor, S. (2025). Curcumin-loaded maltodextrin-based proniosomes potentially effective against gemcitabine-resistant cholangiocarcinoma. *ACS Applied Bio Materials, 8*(1), 913–930.

Tian, F., Xu, S., Gan, M., Chen, B., Luan, Q., & Cai, L. (2025). Bionic cell wall models: Utilizing TEMPO-oxidized cellulose nanofibers for fucoxanthin delivery systems. *Carbohydrate Polymers, 348*, Article 122850.

Wang, Z., Zhou, X., Sheng, L., Zhang, D., Zheng, X., Pan, Y., Yu, X., Liang, X., Wang, Q., Wang, B., & Li, N. (2023). Effect of ultrasonic degradation on the structural feature, physicochemical property and bioactivity of plant and microbial polysaccharides: A review. *International Journal of Biological Macromolecules, 236*, Article 123924.

Wilson, B. K., & Prud'homme, R. K. (2021). Nanoparticle size distribution quantification from transmission electron microscopy (TEM) of ruthenium tetroxide stained polymeric nanoparticles. *Journal of Colloid and Interface Science, 604*, 208–220.

Wu, D. D., Tan, Y., Cao, Z. W., Han, L. J., Zhang, H. L., & Dong, L. S. (2018). Preparation and characterization of maltodextrin-based polyurethane. *Carbohydrate Polymers, 194*, 236–244.

Xiao, H., Zhao, J., Fang, C., Cao, Q., Xing, M., Li, X., Hou, J., Ji, A., & Song, S. (2020). Advances in studies on the pharmacological activities of fucoxanthin. *Marine Drugs, 18*.

Xie, F., Liu, X., Liu, N., Feng, X., He, Z., Din, Z.-u., Cheng, S., Luo, Y., & Cai, J. (2024). Effect of degree of substitution of octenyl succinate on starch micelles for synthesis and stability of selenium nanoparticles: Towards selenium supplements. *International Journal of Biological Macromolecules, 280*, Article 135586.

Xu, H., Ma, Q., Qiu, C., Wang, J., Jin, Z., & Hu, Y. (2024). Encapsulation and controlled delivery of curcumin by self-assembled cyclodextrin succinate/chitosan nanoparticles. *Food Hydrocolloids, 157*, Article 110465.

Yang, M., Wei, Y., Ashokkumar, M., Qin, J., Han, N., & Wang, Y. (2020). Effect of ultrasound on binding interaction between emodin and nanoparticles casein and its microencapsulation at various temperatures. *Ultrasonics Sonochemistry, 62*, Article 104861.

Zhang, Z., Zihao, W., & Xue, C. (2024). Delivery systems for fucoxanthin: Research progress, applications and future prospects. *Critical Reviews in Food Science and Nutrition, 64*(14), 4643–4659.

Zhao, Y., Liu, J., Zhang, S., Wang, Z., Jia, H., Oda, H., & Li, R. (2022). Fabrication and characterization of the H/J-type aggregates astaxanthin/bovine serum albumin/chitosan nanoparticles. *International Journal of Biological Macromolecules, 223*, 1186–1195.

Zhao, S., Tian, G., Zhao, C., Lu, C., Bao, Y., Liu, X., & Zheng, J. (2018). Emulsifying stability properties of octenyl succinic anhydride (OSA) modified waxy starches with different molecular structures. *Food Hydrocolloids, 85*, 248–256.

Zhao, Y., Zhi, J., Huang, S., Zhang, X., Kim, Y.-R., Xu, Y., Wang, D., & Luo, K. (2022). Fabrication of starch/zein-based microcapsules for encapsulation and delivery of fucoxanthin. *Food Chemistry, 392*, Article 133282.